Tribology International 175 (2022) 107782

Contents lists available at ScienceDirect

Tribology International

journal homepage: www.elsevier.com/locate/triboint

Detailed characterization of aeration in lubricating oils by an ultrasonic approach

Che Zhan [a], A. Saint-Jalmes [b], M. Receveur [a], H. El Bahi [c], F. Rondelez [d], V. Leroy [a,*]

[a] Laboratoire Matiere et Systemes Complexes, UMR 7057, Univ. Paris Cité, CNRS, Paris, France
[b] Institut de Physique de Rennes, UMR 6251, Univ. Rennes, CNRS, Rennes, France
[c] Centre de Recherche de Solaize (TotalEnergies), Solaize, France
[d] Laboratoire de Thermodynamique et Energetique des Fluides Complexes et Reservoirs, UMR 5150, TotalEnergies-CNRS-UPPA, Pau, France

ARTICLE INFO

Keywords:
Lubricants
Aeration

ABSTRACT

Lubricating oils get aerated during their use, reducing their efficiency and stability. Deaerating agents are generally added to reduce aeration. Understanding the mechanisms by which these additives set the gas fraction in oil is crucial for the development of optimal formulation. Here we present experiments performed on a Flender test apparatus in which ultrasonic probes are incorporated. We present the technique and demonstrate that it provides the gas volume fraction but also information on the bubble size during the aeration process. Thanks to this measuring technique, new insights on the dynamics of both aeration and de-aeration are gained. As an example, we show how these parameters are affected by the presence of four different additives in a specific reference oil.

1. Introduction

Gas entrainment is hardly preventable when dealing with complex liquid flows having a free liquid–gas interface. This is especially relevant for lubricating oils in mechanical motors. Due to the high rotation rate, the gear is able to incorporate a significant amount of air (up to 15%). Beyond changing the oil turbidity and color, the incorporated gas increases the viscosity [1,2], degrades the stability and can modify the required power to operate pumps or turbines. Previous experiments have shown that entrained air bubbles in crankcase oils and in journal bearings significantly modify the bearing wear [3,4]. This is becoming more and more relevant in the automotive industry [5], where the gear rotation speeds can be as high as 12 000 rpm (rotation per minute), thus possibly leading to even stronger air entrainment, and increased churning losses [6].

Engineers have developed standard technical tests to measure the amount of gas incorporated into an oil, such as the "Impinger Air Release" test [7] or the Flender test [8]. These devices are useful for standardized tests, and help to sort the different formulations. Still, these approaches are limited, with some drawbacks mainly due to the absence of measurements during the dynamical aeration. Even more importantly, the existing methods focus on the gas fraction (mostly by optical means, and after the aeration process), and do not provide measurements of the bubble sizes. Such missing pieces prevent an accurate description of what sets the aeration and deaeration features. Indeed, in the case of the printing industry, where the rotation of the shaft can reach up to 8000 rpm, the importance of knowing not only the aeration level, but also the air bubble size, has been pointed out in modeling of bearing performance [9]. For deaeration also, *i.e.*, when the bubbles escape by gravity, as the rising speed of a bubble scales like its radius to the square it is important to determine the impact of the formulation on the average size of the bubbles.

The question of how the formulation of a liquid impacts its ability to stabilize gas bubbles is still the subject of an active research. Recent results on mixtures of liquids emphasized the roles of evaporation [10,11] and "non-linear" surface tension of mixtures [12]. Regarding the additives, a distinction has been proposed between oils containing, or not, silicone-based additives [13]. With silicone, the incorporated amount of gas is low, but the deaeration – after the entrainment process – is usually slow. Oppositely, additives without silicone incorporate more gas, but this gas takes less time to vanish in static conditions. It has been claimed that the differences in the deaeration dynamics could be related to the interfacial layer adsorbed at the bubble surface, leading to density [13] or Marangoni [14] effects. However, discriminating between the different possible mechanisms requires that the experiments are performed at fixed bubble radii.

Ultrasonic waves are well suited to study bubbly liquids since their propagation in liquids is very sensitive to the presence of bubbles [15]. Therefore, our objective was to couple ultrasound techniques to an

* Corresponding author.
E-mail address: valentin.leroy@u-paris.fr (V. Leroy).

https://doi.org/10.1016/j.triboint.2022.107782
Received 23 April 2022; Received in revised form 16 June 2022; Accepted 12 July 2022
Available online 26 July 2022
0301-679X/© 2022 Elsevier Ltd. All rights reserved.

aeration apparatus, and to determine what information can then be obtained during the aeration process. Note that this study is limited to aeration only. Foaming was disregarded, as it was found to be low for the oils we used (the incorporated gas fraction remained always below about 15%).

Below, we start by describing the experimental setup for oil aeration, including the ultrasonic probes, as well as optical tools for comparisons. For these experiments, five different oil formulations have been selected, on which complementary interfacial and bulk characterizations have been independently performed. Then we present the measurements and the data analysis. We show how the gas fraction, bubble size, and the time required to reach a steady state of aeration can be extracted from the ultrasonic data. Once these important parameters have been identified, the 4 additives used in our experiments can be separated in 2 different groups, and we propose a simple model to rationalize these observations.

2. Material and methods

2.1. Oils

Five different samples were used in the study: a reference oil that led to moderate aeration in a standard Flender test, and four other samples prepared by adding deaerating additives to this oil. The reference oil (Sample A) was a class III (American Petroleum Institute classification) mineral oil. Its physical properties were: density $\rho = 825.5\ \mathrm{kg/m^3}$, kinematic viscosity $\nu = 34.8\ \mathrm{mm^2/s}$, speed of sound (at 5 MHz) $c = 1.43\ \mathrm{mm/\mu s}$ and attenuation $0.02\ \mathrm{m^{-1}}$, at 25 °C. The temperature dependency of these parameters is important to know, because the experiments lead to non-negligible heating (up to 5 °C). Variations could be considered as linear in the 20–30 °C range: $-0.64\ \mathrm{kg/m^3/K}$ for ρ, $-1.5\ \mathrm{mm^2/s/K}$ for ν, $-2.9\times10^{-3}\ \mathrm{mm/\mu s/K}$ for c, and close to zero for the attenuation.

Samples B, C, D and E were obtained by adding different deaerating additives to oil A. All these additives are used in commercial products. The additives in B, C and D are based on polysiloxane chains: B contains pure polysiloxane, C polysiloxane and SiO2 particles, and D ramified alcoxylated polysiloxane. The molar mass of the polysiloxane chains are also different: 150 g/mM for B, 70 g/mM for C and 25 g/mM for D. The additive in E is a polyacrylate chain, of unknown molar mass. Among a larger range of oils and additives tested, we selected these five samples as they clearly illustrate the purpose of this article, while corresponding to the best trade-off between simple model systems and realistic ones relevant for the industrial applications.

In all cases, the concentrations are low enough (less than 0.05%) to consider that, except for the surface tension, the above physical properties remain the same as for sample A. Note also that once added into the reference oil, these additives are dispersed as globules of micrometer sizes.

As we are interested in aeration properties, the air–oil interfaces have to be characterized, especially to determine if the additives adsorb at the interface. In a motor, due to the gear rotation, the aeration and bubble creation processes are fast; therefore, we focus on measuring the effect of the additives on surface tensions at comparable time scales. The surface tensions were measured at 0.1 s and 1 s after the creation of a fresh interface, by using the maximal bubble pressure technique (Sinterface BPA-1). For measurements over longer times (up to minutes) a pendant drop apparatus (Tracker - Teclis) was used.

The results are shown in Table 1 and Fig. 1. It is found that all the additives decrease the surface tension, typically by a few mN/m, meaning that some significant adsorption occurs at the interface. After 1 s, the decrease is stronger for sample B and C, and this trend is maintained at longer times. The data at 1 min and longer time shows that the equilibrium is typically obtained within the first minute.

The pendant drop setup can also be used to perform oscillatory tests, providing measurements of the dilational interfacial elasticity.

Table 1
Physico-chemical properties of the samples, surface tension γ and surface elasticity E.

Sample	γ at 0.1 s (mN/m)	γ at 1 s (mN/m)	γ at 1 min (mN/m)	E (mN/m)
A	32	29.6	29	<5
B	28.5	25	23.5	11.4
C	30.2	25.8	24.8	20
D	31.7	29.1	28.5	<5
E	29.5	27	26	<5

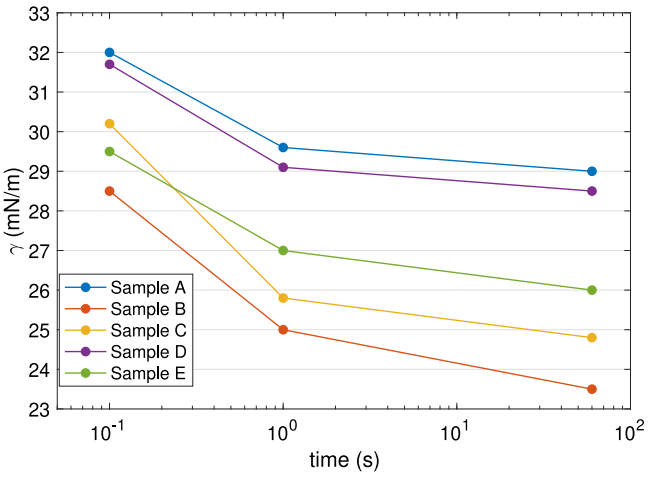

Fig. 1. Surface tension as a function of time for the five samples.

Results are given in the last column of Table 1 for a frequency of 1 Hz and a deformation amplitude of 5%: sample B and C show an elastic behavior, but it is not the case for the other samples A, D and E. It means that in these latter cases, the molecules present at the air–oil interface exchange with the bulk surface sufficiently rapidly to adapt to the mechanical solicitation at 1 Hz. Another way of saying is that they are more oil-soluble than the additives in B and C.

2.2. Experimental setup

The setup is based on the Flender test [8], but with a simpler mechanical setting, and an extension for ultrasonic measurements. As shown in the drawings of Fig. 2, we use only one gear (instead of two), half-immersed in oil and entrained by a motor. Because ultrasounds are strongly attenuated when bubbles are present, it is not possible to measure ultrasonic transmission through the entire length of the casing. To solve this issue, we have added a small extension on one face of the casing (see Fig. 2). This extension has a thickness of 5 mm, allowing us to measure the transmission of ultrasounds through the bubbly oil. A natural question is whether the aerated oil we probe in this extension is representative of the whole sample. One could imagine that the population of bubbles visiting the extension is not the same as in other parts of the casing. Although we cannot totally rule out this scenario, the high turbulence induced by the rotation of the gear leads to a quite homogeneous flow, and visual inspection during the experiments has confirmed the presence of many bubbles flowing in the extension.

In the following we give details on the different aspects of the setup: mechanics (gear and motor), temperature probe, optical measurements, and ultrasonic measurements.

2.2.1. Gear and motor

The casing is made of acrylic (PMMA) walls and has a section of $13 \times 13\ \mathrm{cm^2}$ for a height of 15 cm. The gear has a diameter of 10 cm, a height of 2.5 cm, and 38 teeth. It was 3D-printed in polylactic acid

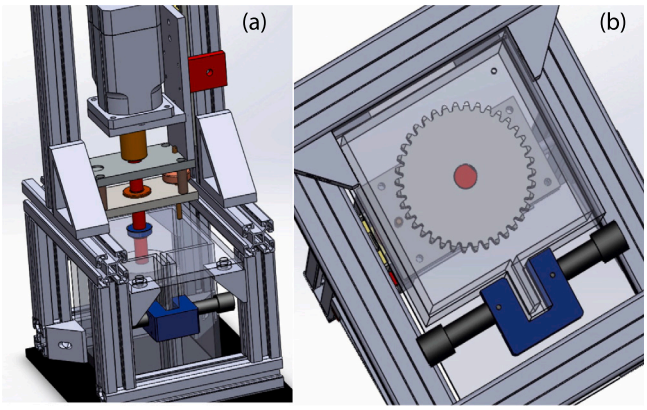

Fig. 2. 3D drawings of the setup. General (a) and bottom (b) views. The ultrasonic extension is clearly visible on the bottom view. It consists of two transducers (dark gray cylinders) held by a clip (in blue) on the 5 mm-wide chamber of the casing, allowing for the measurement of the ultrasonic transmission through the aerated oil. (For interpretation of the references to color in this figure legend, the reader is referred to the web version of this article.)

(PLA). The motor (Transtechnik) has a nominal torque of 1.65 Nm and a maximal speed of 6000 rotations per minute (rpm). Its controller allows for a precise control of the speed and a measurement of the applied torque. Note that with our gear of 10 cm in diameter, the tangential speed at 6000 rpm is equivalent to that of a 5 cm gear at 12 000 rpm. We are thus close to the conditions encountered in real applications, the typical diameter of a gear in automotive being 5 cm. A typical run consisted in an accelerating phase of duration t_0, followed by a period Δt at rotation speed Ω, ended by a decelerating phase, of duration t_1. Fig. 3a shows an example of the torque applied by the motor (solid black line) for a run with $t_0 = 0.1$ s, $\Delta t = 1$ min, $t_1 = 5$ s with a speed of $\Omega = 2000$ rpm in oil A. The light gray curve on the same graph shows the torque measured for the same run in air. The difference between the two measurements, in oil and in air, allows us to estimate the churning losses, which is $\mathcal{P} = 33.5 \pm 6$ W in this example.

Runs at speeds of $\Omega = 500$, 1000, 2000 and 4000 rpm were done for each oil sample, and were repeated at least twice.

2.2.2. Temperature

The temperature is measured by a type K thermocouple, placed in the "ultrasonic extension" and close to the region where the ultrasonic transmission is measured. Fig. 3a shows (blue line) the temperature evolution in our example run: it increases by approximately 1.5 °C during the rotation period, and slowly decreases after.

Note that there is no heating or cooling device. The initial temperature for a run is either the room temperature or the temperature reached during the previous run.

2.2.3. Ultrasonic measurements

The lateral extension for ultrasonic measurements is 3 cm long and 0.5 cm wide. Two ultrasonic transducers (Olympus, 5 MHz central frequency, 0.64 cm diameter) are placed on the walls, facing each other, and a thin layer of gel (Olympus) insures a good transmission of the ultrasonic signal. A pulser (Sofranel, DPR 300) excites one of the transducers with a short electric pulse, thus generating an acoustic signal that travels through the first wall, the oil, and the second wall, to be received by the other transducer, which converts it into an electric signal recorded by an oscilloscope (TiePie Handyscope HS5). We apply a Fourier transform to the acquired pulse, to extract the 5 MHz component. The transmission, T, is obtained by dividing this 5 MHz component by a reference measurement, acquired in the absence of bubbles (before the rotation of the gear). Note that T is a complex quantity, with a real and an imaginary part. For the analysis (see

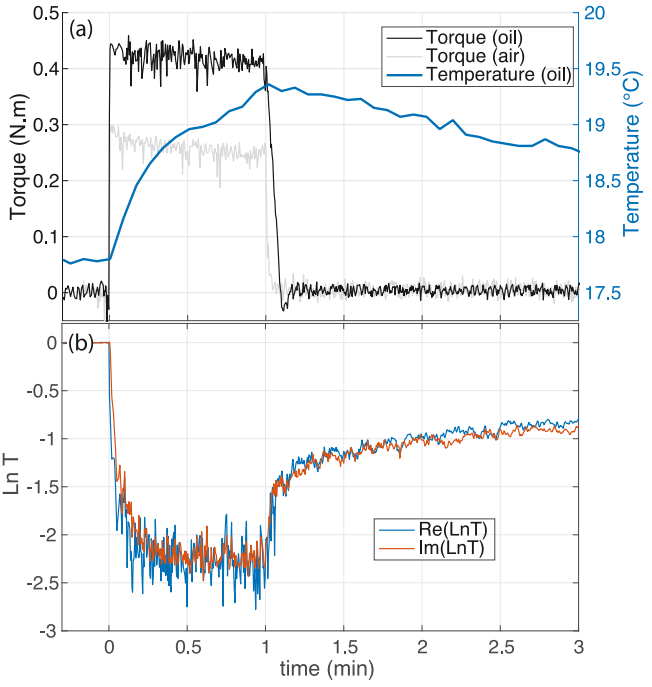

Fig. 3. Illustrations of the data acquired during a run, here for 1 min of rotation at $\Omega = 2000$ rpm in oil A. (a) Torque and temperature as functions of time. (b) Logarithm of the ultrasonic complex transmission at 5 MHz. (For interpretation of the references to color in this figure legend, the reader is referred to the web version of this article.)

Section 2.3.2), a convenient quantity is LnT, the logarithm of T. The real part (ReLnT) is an indication of how much attenuating the bubbly oil is for ultrasounds, and the imaginary part (ImLnT) depends on the velocity of ultrasounds in the bubbly oil. For the imaginary part, corrections are applied to take into account the effect of temperature on the ultrasonic velocity in the oil (typically 0.2 rad for a 1 °C increase).

Fig. 3b shows how the real and imaginary parts of LnT evolve during the run. We note that both ReLnT and ImLnT decrease as soon as the gear starts to rotate, reaching a stationary value of the order of −2.2 in less than 30 s. When the motor stops, both quantities suddenly increase, and then slowly evolve. All these changes in the ultrasonic transmission can be interpreted in terms of aeration of the oil: bubbles are quickly generated by the rotation of the gear, reaching a stationary regime within 30 s, and when the motors stops, some bubbles escape quickly, but many of them are still present in the oil and will slowly escape, driven by gravity. It means that ultrasounds can give insight on both the turbulent mixing and the static deaeration phases. We will show in Section 2.3.2 that quantitative information on the number of bubbles and their size can be obtained by a careful analysis of the ultrasonic data.

2.2.4. Imaging

As for the standard Flender test, the level of oil is measured with a ruler glued on the wall. A camera takes a picture every 2 s. Fig. 4 shows examples of images acquired before and just after the run. From these images we can estimate the total volume of air entrapped in the oil.

2.3. Data analysis

In this section we give some details on the data analysis for images and ultrasonic acquisitions.

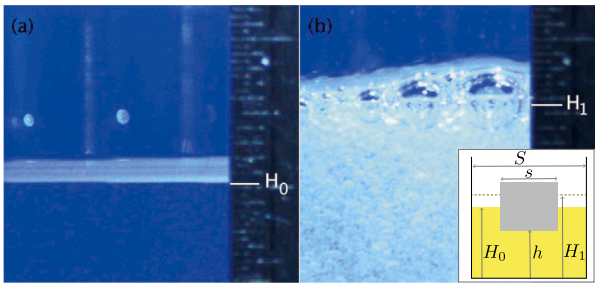

Fig. 4. Examples of images acquired before (a) and just after (b) the rotation of the gear, in oil A at $\Omega = 2000$ rpm. The initial height of oil H_0 is increased to H_1 because of the air entrained. The inset shows the geometrical parameters needed for calculating the air volume fraction from this change of oil level (Eq. (1)). Here we find $H_0 = 8.02$ cm and H_1 between 8.42 and 8.58 cm, leading to $\Phi_{opt} = 3.3 \pm 0.5\%$.

2.3.1. Image analysis

The volume fraction of air in the oil when the motor stops, noted Φ_{opt}, is estimated by comparing optically the level of oil before the run (H_0) and after the run (H_1). Because the volume occupied by the gear in the casing is not negligible, Φ_{opt} does not reduce to $1 - H_0/H_1$. With the geometrical parameters noted in the inset of Fig. 4, it can be shown that the volume fraction of air is given by

$$\Phi_{opt} = \frac{H_1 - H_0}{H_1}\left[1 + \frac{hs}{H_1(S-s)}\right]^{-1}. \quad (1)$$

In our case, it brings a correction factor of the order of 0.58 to the simple formula.

The main source of uncertainty in the determination of Φ_{opt} is the measurement of H_1, because the level of the oil is not always clearly defined after the run due to the presence of a froth of large bubbles. This is illustrated in Fig. 4b, for the case of oil A at 2000 rpm. The froth was more or less important, depending on the formulation and the speed. Its presence led to uncertainties of the order of $\pm 1\%$ for some samples.

2.3.2. Ultrasonic analysis

Presence of bubbles in a liquid is known to drastically change its acoustical properties. In practice, the bubbly liquid can be considered as an effective medium, with effective attenuation and velocity that depend on the population of bubbles. The Independent Scattering Approximation (ISA) has been found to be a reliable theory for modeling the effective acoustical properties for bubbly liquids, in the limit of low to moderate concentrations of bubbles [16]. In this work, we use the ISA to extract information on the bubbles from the 5 MHz transmission measurements. Details on the model and how to use it for monitoring a bubble population can be found in [15]. Therefore, we only give here an overview of the procedure.

Since only two quantities are measured (ReLnT and ImLnT), it is not possible to reconstruct a complete histogram of the bubble sizes. Hypothesis need to be made. The first one is to assume that the population of bubbles follows a lognormal law. Under this condition the density number of bubbles is given by

$$n(r) = \frac{n_0}{r\epsilon\sqrt{2\pi}} \exp\left[-\frac{[\ln(r/r_0]^2}{2\epsilon^2}\right], \quad (2)$$

with n_0 the total number of bubbles per unit volume, r_0 the median radius, and ϵ the polydispersity. The volume fraction of bubbles is then given by $\Phi = \int n(r) 4\pi r^3/3 dr = (4\pi n_0 r_0^3/3)\exp(9\epsilon^2/2)$. It is important to note that our choice of a lognormal distribution is not based on a particular mechanism for the bubbles formation. It is just a convenient assumption to extract the median radius and the width of the distribution.

Fig. 5 gives the analysis of Fig. 3b's data in terms of air volume fraction (Φ) and bubble median radius (r_0) as function of time. Here

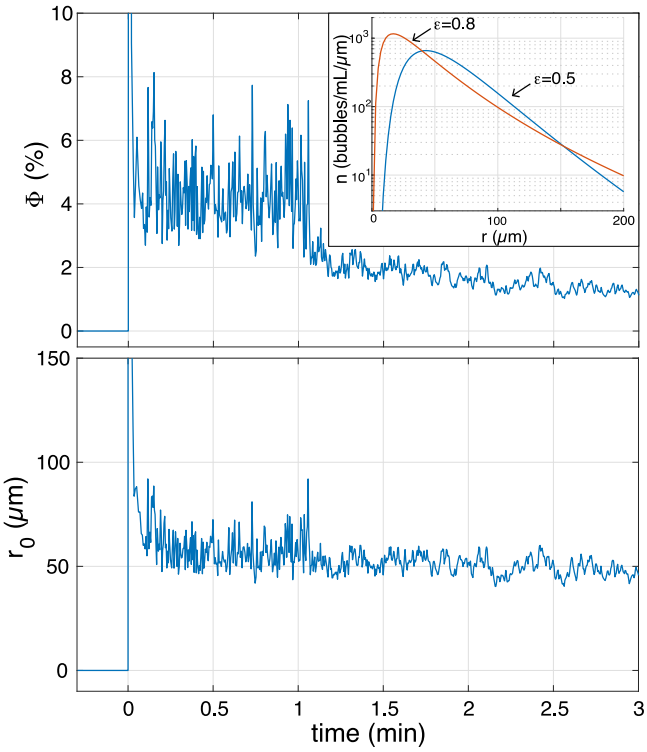

Fig. 5. Air volume fraction (Φ) and bubble median radius (r_0) obtained by analyzing the ultrasonic data from Fig. 3b, assuming that the polydispersity is 0.5. The inset shows the distributions one obtains one minute after the start of the motor, when assuming a polydispersity of 0.5 (blue) or 0.8 (red). (For interpretation of the references to color in this figure legend, the reader is referred to the web version of this article.)

Table 2
Variations of the parameters of the distribution according to the hypothesis on its width ϵ, for the data of Fig. 3 at $t = 1$ min.

ϵ	r_0 (μm)	Φ (%)	R_{min} (μm)	R_{max} (μm)
0.20	73	3.2	49	109
0.35	64	3.5	32	130
0.50	53	4.1	20	144
0.65	41	4.9	11	150
0.80	29	6.1	6	145

we have assumed that the polydispersity of the distribution is 0.5. The inset of Fig. 5 shows, in blue, the corresponding distribution at $t = 1$ min. Other values of ϵ, however, could have been chosen and this is a limitation of the analysis. The inset shows how the distribution is affected if $\epsilon = 0.8$: the distribution is shifted towards smaller bubbles. There is clearly an uncertainty on the smallest bubbles present in the liquid.

Instead of using r_0 and ϵ, another way to characterize the bubble distribution, is to look at R_{min} and R_{max} defined by

$$R_{min} = r_0 \exp(-2\epsilon), \quad (3)$$

$$R_{max} = r_0 \exp(+2\epsilon). \quad (4)$$

These two radii give an estimate of the minimal and maximal sizes in the distribution: 95% of the bubbles are on the [R_{min} - R_{max}] interval. As shown in Table 2, R_{max} is much less sensitive than r_0 to the choice of ϵ. Therefore this parameter is a robust observable for the typical size of the bubbles in the oil.

To take into account the uncertainty related to the polydispersity, we have treated the ultrasonic data using different values for ϵ. Visual observations for some experiments at low Ω showed than ϵ was of the order of 0.65 (see Appendix). We assumed that the polydispersity

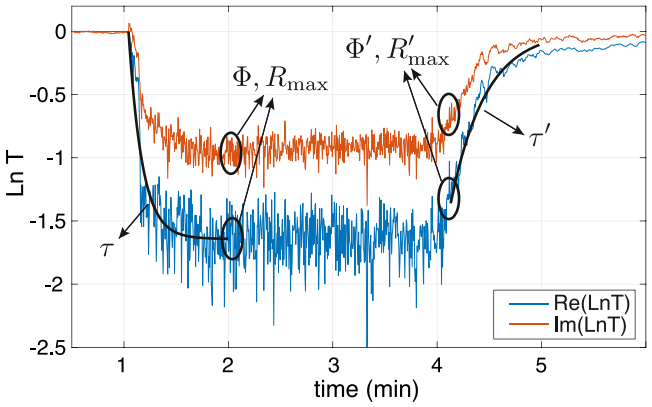

Fig. 6. Illustration of the 6 parameters extracted from the ultrasonic measurements, here for sample E at 1000 rpm. Φ, R_{max} and τ provide information on the aeration phase, while Φ', R'_{max} and τ' are used to characterize the deaeration phase.

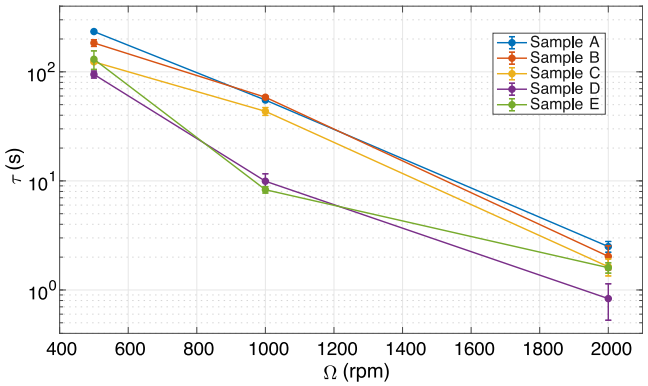

Fig. 7. Time for reaching a steady state (τ) as a function of the speed of rotation (Ω) for the five oils. We see that formulations D and E aerated faster than the other oils.

remained in the same range for other speeds of rotation. This is our second hypothesis. Note, however, that we did not take a strict hypothesis of $\epsilon = 0.65$. The analysis of the ultrasonic data was conducted for values of ϵ ranging from 0.45 to 0.85, leading to different results in terms of Φ and R_{max}. We then considered the mean values and standard deviations of all those results. Errorbars were estimated by taking into account both the replicas and the sensitivity to the polydispersity hypothesis.

2.3.3. Parameters for air bubbles characterization

In total, 7 different parameters can be used for characterizing the aeration (see Fig. 6), 6 from the ultrasonic results and one from the optical analysis:

- τ is the characteristic time of the dynamic aeration, evaluated by fitting the first decrease of ReLnT with an exponential law,
- Φ gives the air volume fraction when the stationary regime of turbulent mixing is reached
- R_{max} is the size of the large bubbles in the stationary regime,
- Φ' is the air volume fraction when the motor stops rotating, from the ultrasonic analysis
- Φ_{opt} is the air volume fraction when the motor stops, as obtained from image analysis.
- R'_{max} is the size of large bubbles when the motor stops
- τ' is the characteristic time of the static deaeration, evaluated by fitting ReLnT after the motor stops.

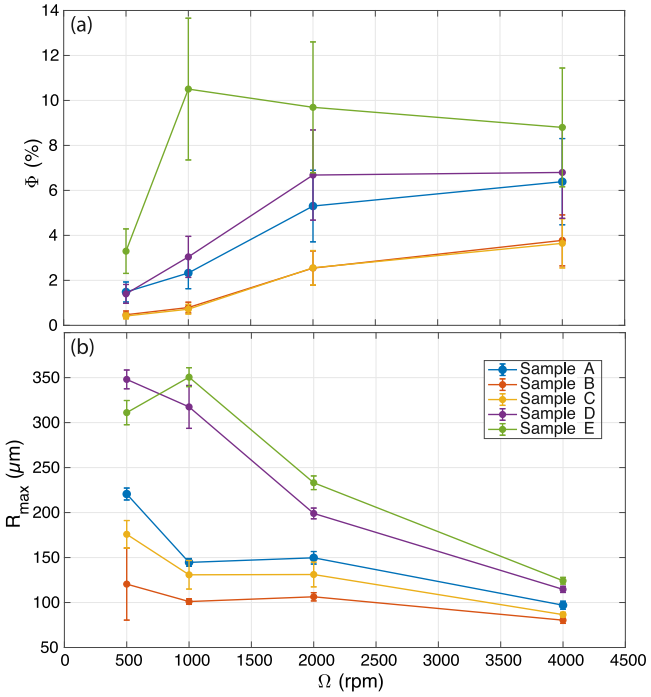

Fig. 8. Φ (top) and R_{max} (bottom) as functions of Ω for the five oils, in the steady state of turbulent mixing. There is a clear effect of the formulation: B and C tend to entrap less air, with small bubbles, while D and E have larger bubbles and more air.

3. Results

In this section, we present the results obtained with the different samples, insisting on the differences and similarities that appear from one formulation to the other. We look at three different phases of a run: the turbulent mixing, the moment the motor stops, and the phase of static deaeration.

3.1. Phase of turbulent mixing

The ultrasonic measurements offer the unique advantage of giving information on the aeration process in real time, when the gear is rotating. The first piece of useful information is the time τ necessary for reaching a steady regime. In Fig. 3b for example, we see that less than 30 s is enough for sample A to be in a steady state at 2000 rpm. Fig. 7 shows the results of τ as a function of Ω for the five oil samples. We find that τ decreases with Ω, meaning that the steady state is reached earlier when the motor rotates quickly. Note that for $\Omega = 4000$ rpm the phenomenon is too fast to be resolved by the ultrasound measurements, meaning that at this speed τ is lower than 0.5 s.

Interestingly, we can see a difference between the five formulations: samples D and E tend to aerate faster than the other oils. This is a first indication that formulation has an impact on the aeration process. Further insight is given by the results on Φ and R_{max}, as reported in Fig. 8. The general trend is to have more air and smaller bubbles, when the speed increases. But we clearly see that samples D and E entrap more air than the reference oil A, and with larger bubbles. On the contrary, samples B and C entrap less air, with smaller bubbles.

3.2. When the motor stops

Fig. 9 shows the result of the optical analysis, which gives the volume fraction of air in the oil when the motor stops rotating. A similar hierarchy of aeration as in Fig. 8a is found: sample E is the most aerated, D and A have comparable levels, while B and C entrap less air. The levels of aeration, however, are always less when the motor

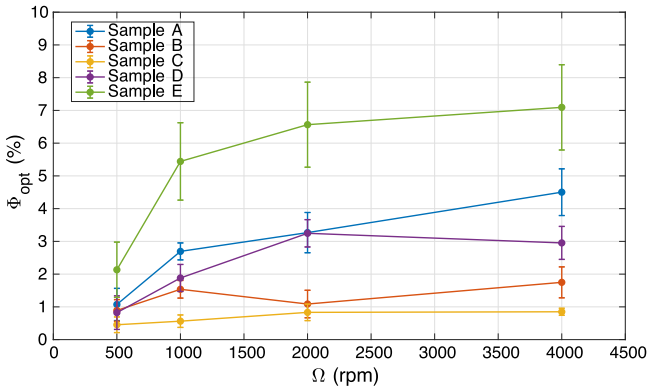

Fig. 9. Volume fraction of air as a function of Ω as given by the analysis of the images taken within 2 s after the motor has stopped. The levels of aeration are smaller than in the mixing phase (see Fig. 8a).

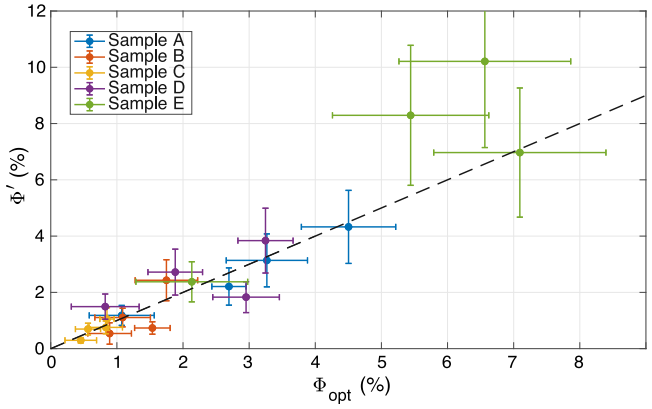

Fig. 10. Aeration when the motor stops as measured acoustically (Φ') and optically (Φ_{opt}). The agreement is reasonable, which suggests that the bubbles visiting the 5 mm extension are well representative of the total population of bubbles.

stops than in the steady regime. At 1000 rpm for example, sample E is aerated at 10% when the gear rotates, and only 5.5% when it stops. For sample C, at the same speed, it goes from 1% to 0.5%. This is not surprising, given the short time necessary for the steady state to be reached: it means that during the deceleration phase, the level of aeration has time to adapt to the changing speed. In other words, we cannot consider that the optical measurement at rest is representative of the amount of air entrapped during the mixing phase, because the motor does not stop quickly enough. We checked that the aerations evaluated by optics and acoustics were compatible: Fig. 10 shows that Φ' and Φ_{opt} are in a reasonable agreement, within the errorbars. This is also an indirect confirmation that the population of bubbles probed by the ultrasounds in the extension is well representative of what is going on in the whole casing.

3.3. Phase of deaeration

When the motor stops, the bubbles rise and the amount of air entrapped decreases with time. We can monitor how quickly the oil deaerates by looking at τ'. As shown in Fig. 11, there is a strong correlation between τ' and the radius of the bubbles entrapped during the mixing phase: the larger the bubbles, the shorter the deaeration time. It can be understood by the fact that larger bubbles rise faster than smaller ones, as discussed in the next section.

Note that there are some exceptions in Fig. 11: for samples D and E at high speed, the bubbles are small but τ' remains small. For instance at $\Omega = 4000$ rpm for sample D, we find that R'_{max} is of the order of

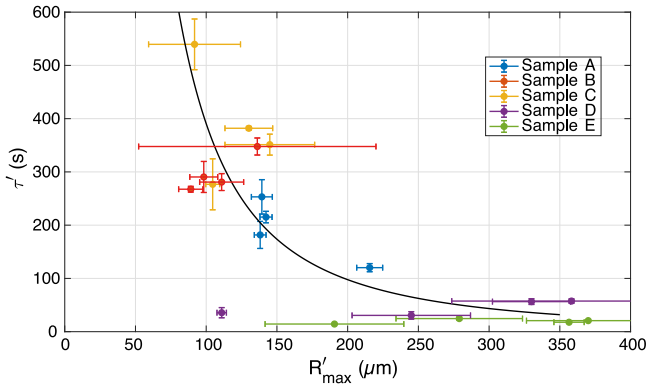

Fig. 11. Deaeration time τ' as a function of R'_{max}, the radius of the larger bubbles in the oil, when the motor stops. We find that the larger the bubbles the quicker the deaeration process. The solid line is a guide for the eyes (not a fit) of a $1/x^2$ law.

100 μm, while the deaeration time is very low, of the order of 30 s. We think that this is due to the presence of large bubbles that are not well detected by the ultrasounds. As shown in the Appendix, the lognormal hypothesis is reasonable for capturing the general shape of the distribution, but fails at taking into account the few very large bubbles that are entrapped, especially for samples D and E. These large bubbles might explain the short deaeration time, as they can pull up all the bubbles when they quickly rise to the surface.

4. Discussion

Deaerating additives are expected to modify the amount of air entrained in the oils, this is what they were designed for. Our ultrasonic measurements have shown that they actually change the gas volume fraction, but also, and even more importantly, the bubble size: it can vary by a factor of 3 from one formulation to the other.

This point brings a simple explanation to the differences noticed in the speeds of deaeration. Marangoni [14] and density effects [13] probably exist, but they cannot quantitatively explain a factor 10 in the deaeration time, as observed in our data (see Fig. 11). A factor 3 on the radius, on the other hand, is consistent with this observation, as the rising speed of a bubble in a viscous fluid is expected to be proportional to R^2. Thus, it seems that understanding the effect of the formulation on the deaeration time reduces to understanding how the formulation affects the size of the bubbles reached in steady state during the mixing phase.

It is clear from Fig. 8 that the additives in Samples B and C lead to the entrapment of smaller bubbles, whereas the additives in Samples D and E yield larger bubbles. A natural question is then to wonder whether the additives affect the number of bubbles entrained by the gear.

In our analysis of the ultrasonic data, we have calculated the total volume fraction of air. Another approach is to consider the number of bubbles per unit volume, n_0, which is given by

$$n_0 = \frac{3\Phi}{4\pi R_{max}^3} \exp[6\epsilon(1-3\epsilon/4)], \quad (5)$$

still within the assumption of a lognormal distribution. Fig. 12 shows the results in terms of n_0 for the different samples, with errorbars to take into account our uncertainty about the actual polydispersity. When Ω goes from 500 to 4000 rpm, n_0 increases by about two orders of magnitude.

At the lowest rotation speeds, there are significant differences between the deaerant additives. The additives in oils C, D and E tend to reduce the number of bubbles compared to the sample A without additives, with a stronger effect for sample D. For sample B, the number of bubbles remains more or less the same as in the reference sample.

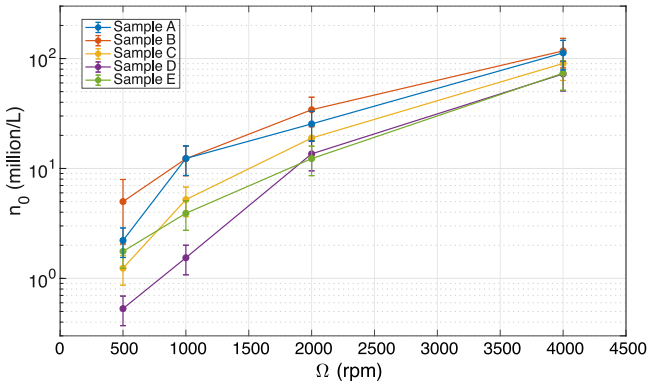

Fig. 12. Number of bubbles per unit volume, n_0 (in million per liter), as a function of Ω, for the different samples.

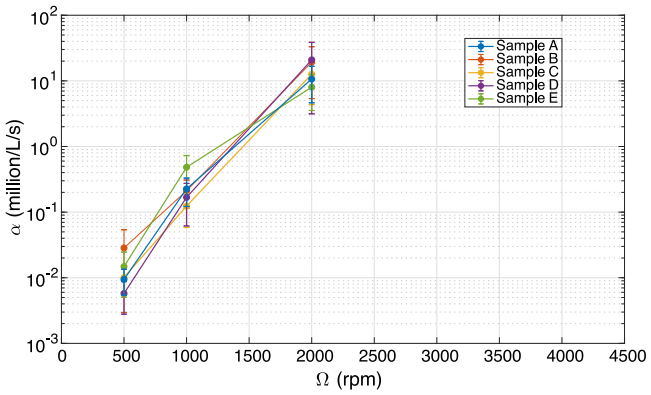

Fig. 13. Rate of bubble production, α, as a function of Ω, for the different samples.

One should note that the differences between the samples decrease as the rotation speeds increase.

Analyzing the data in terms of (n_0, R_{max}) instead of (Φ, R_{max}) offers the opportunity to interpret the experimental results in the framework of a simple model. Let us assume that, during the rotation of the gear, the change in the number of bubbles during a short time dt is given by

$$dN = +\alpha dt - \beta N dt, \tag{6}$$

where α is the number of bubbles per unit of volume and per unit of time created by the rotation of the gear, and β the fraction of bubbles per unit of time that is lost at the surface. This is a crude model that does not consider polydispersity: only one class of size is considered. A more elaborated model would include different classes of size, and processes for exchanges from one class to the other, by coalescence and breakups. However, we emphasize that this 2-parameter model contains the most important physical ingredients that dictate the fate of a population of bubbles: its production and destruction rates, α and β.

With an initial condition of no bubble, integrating Eq. (6) leads to the following law:

$$N(t) = \frac{\alpha}{\beta}\left(1 - \exp(-\beta t)\right). \tag{7}$$

It thus predicts that the transient regime is governed by the destruction rate β, and that in steady state, the number of bubbles per liter is given by $n_0 = \alpha/\beta$.

At this stage, it is tempting to identify $1/\beta$ with our measurement of the time necessary to reach the steady state, τ. The model thus suggests that the decrease of τ for the oils with additives (see Fig. 7) indicates that bubbles disappear more easily. This is what is expected for deaerating agents: additives are supposed to act at the scale of the thin liquid films [17–20], provoking their rupture and hence facilitating the burst of bubbles when they reach the surface. Another consequence of an easy rupture of the films is to favor the coalescence of the air bubbles. This may explain why the two formulations with the lowest values of τ (D and E) are also the ones that entrap the largest bubbles. Note, however, that this scenario gives no clue to explain why the volume fraction of gas is higher in these two samples: coalescence events change the sizes and numbers of bubbles, but not the total volume of gas.

If we consider that $\beta = 1/\tau$, we can use our experimental data to estimate α, the rate of bubble production: $\alpha = n_0/\tau$. The result is shown in Fig. 13, limited to a maximum velocity of $\Omega = 2000$ rpm because for higher speeds the transient regime is too quick to be captured by our ultrasonic technique. It is worth noting that α depends strongly on Ω: it increases by 3 orders of magnitude when Ω is simply multiplied by a factor 4, reaching a production rate of several millions of bubbles per liter and per second, for $\Omega = 2000$ rpm. Interestingly, no clear trend emerges in Fig. 13 when comparing the different samples, suggesting that the formulation has a limited impact on α. This is remarkable because our estimate of α is obtained by dividing two quantities, τ and n_0, that were found to depend on the formulation (see Figs. 7 and 12). It suggests that the differences in n_0 observed in Fig. 12 would mainly be due to differences in bubbles destruction ($\beta = 1/\tau$), not in bubbles production (α). In other words, the additives would affect the disappearance of bubbles but not their rate of production.

Coming back to the volume fraction of air, which is the main parameter of interest for most applications, our simple model suggests the following formulation:

$$\Phi = \frac{4}{3}\pi R^3 \frac{\alpha}{\beta}. \tag{8}$$

It means that Φ depends on three parameters: the rate of production (α), the rate of destruction (β) and the radius of the bubbles (R). Therefore there are three levers one can use to minimize the amount of gas entrapped in oil: (i) reducing the entrapment, (ii) increasing the destruction rate, (iii) decreasing the size of the bubbles.

The size of the bubbles is clearly the most sensitive parameter because it appears with a cubic exponent in the equation. According to our experimental results, the success of the additives used in samples B and C come from their ability to entrain small bubbles. On the other hand, samples D and E entrap large bubbles, which disappear quickly, but not quickly enough to compensate for their large volume. Our results thus suggest that the main effect of the additives is to change the average size of the bubbles during the production stage. About the same number of bubbles is produced (α, see Fig. 13), but not of the same sizes.

Further experiments are needed to identify the mechanisms that could explain these different behaviors. Non-aqueous foams are a fairly recent and complex field of research (see the recent review by Calhoun et al. [21]), with many possible microscopic mechanisms involved. Therefore, at this stage we first want to report the correlations we found between the aeration features and the physico-chemical characterization of the different samples. Regarding the surface tensions, there are small differences (Table 1) but the values are all within the same range. So, if this measurement is the only interfacial characterization available, it is impossible to draw correlations with the aeration behavior and to sort the samples. Still, we can point out that once additives are added, the surface tensions are smaller. On the contrary, we note that the class of "small bubbles" (samples B and C) consists in the only chemical formulations providing interfacial elasticity (see Table 1).

Beyond the interfacial elasticity which correlates well with the aeration behavior, other simple complementary tests performed on the pure additives also show the separation in the same two classes. We have tested how a millimetric drop of the pure additive behave once in

contact with the air–oil interface of the reference oil (sample A). It is found that the oil does not wet the drops of the additives used in sample B and C (polysiloxane), and that these drops do not spontaneously dissolve in the oil. A rather opposite behavior is observed for drops of the additives used in sample D and E (alkoxylated polysiloxane and polyacrylate) : these drops easily spread on the air–oil interface, associated with an efficient dissolution in the oil.

Regarding the value of β and the microscopic mechanisms by which the globules of additives enhance the rupture of thin liquid films, we can only speculate at this stage, comparing our observations to what is known on the different classes of anti-foaming agents in aqueous foams. The fact that a specific feature of our first class of additives (samples B and C) is that a drop of additive is not wetted by the oil, while additives of our second class of additives (samples D and E) easily spread on the air–oil interface recalls the separation between the "bridging–dewetting" and the "spreading" mechanisms already reported for antifoaming agents [19–21]. Indeed, the "bridging–dewetting" mechanism relies on non-wetting globules trapped in the films, and which eventually break them as they thin down. In that case, the addition of solid nanoparticles are known to enhance the dewetting and the film rupture. In the other mechanism, it is required to have additive globules that deform and lay on the surface of the thin film to induce its rupture.

5. Conclusion

We have demonstrated that ultrasound is a convenient tool for probing the population of bubbles generated during an aeration process. It allows time-resolved measurements of both the air fraction and the bubble size *during* the aeration process. Thanks to ultrasound, we can estimate the size of the bubbles, and their production and destruction rates, the three main levers we identified as relevant for lowering the volume fraction of air during the aeration phase. Our modified Flender test could thus be useful for optimizing formulation of deaerating agents for lubricating oils. As well, in recent articles, computational fluid dynamics (CFD) models of lubrication in bearings have been developed, that integrate aeration effects, and eventually provide a better agreement with the data [22,23]. It would then be interesting to couple independent ultrasound measurements of bubble sizes and gas fractions with these numerical developments, to test the validity and improve such numerical solvers.

Our results show that it is worth measuring the size of the bubbles in aeration problems, and not only the total volume fraction of air. By testing four different chemical formulations containing deaerating additives, we showed that such additives systematically have an impact on the size of the entrained bubbles. Some formulations lead to larger bubbles, while others provide smaller ones. The latter case appears more favorable for reducing the total volume fraction of air, but led to a slower deaeration in the static regime. Therefore, for any given application including aeration issues, there must be an optimal chemical formulation, fulfilling the desired requirements. Finding the links between the chemical structure of the additives and their functionality at the macroscopic scale implies to understand how these additives first set the bubble size and gas fraction.

Declaration of competing interest

The authors declare that they have no known competing financial interests or personal relationships that could have appeared to influence the work reported in this paper.

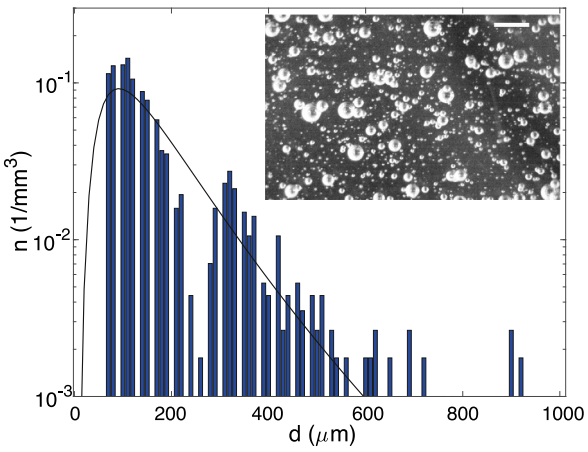

Fig. A.14. Histogram of the bubbles diameters obtained by image analysis. Here for sample D at 500 rpm. Result of the fitting with a lognormal law is shown by the black line. We obtain $R_0 = 85$ µm, $\epsilon = 0.65$ and $\Phi = 1.8\%$. Inset: a typical image. The bar is 2 mm long.

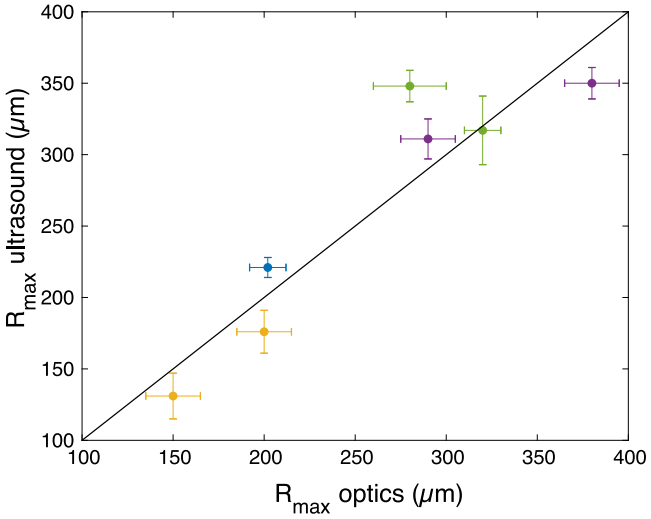

Fig. A.15. Comparison of values of R_{max} obtained by the ultrasonic analysis (y-axis) and the optical one (x-axis), for oil A at 500 rpm (blue symbol) and samples C, D, E at 500 and 1000 rpm. (For interpretation of the references to color in this figure legend, the reader is referred to the web version of this article.)

Appendix. Visual inspection of bubble sizes

For some runs, we used a high magnification objective to observe the bubbles during mixing. With our camera, this was only possible for angular speeds of 500 and 1000 rpm. For higher speeds, the images were too blurred to be analyzed. The observation was done in the extension, slightly below the zone probed by the ultrasounds. Fig. A.14 shows a typical image (inset), obtained for sample D at 500 rpm, one minute after the rotation had started. By analyzing this image, an histogram of the bubble sizes can be obtained. When fitted with a lognormal law, it gives $R_0 = 85$ µm, $\epsilon = 0.65$. With this distribution we obtain $R_{max} = 312$ µm, which is compatible with what is measured with the ultrasonic technique (see Fig. 8). Note that the lognormal law captures well the general shape of the distribution, but it fails at taking the largest bubbles into account. A secondary peak at about 900 µm in diameter is visible on the histogram. It means that the largest bubbles present in the flow are significantly larger than R_{max}. Nevertheless, R_{max} remains a valid parameter for estimating the main part of the distribution.

Fig. A.15 proposes a comparison of the optical and ultrasonic results, in terms of R_{max}, for several samples. A good agreement is obtained.

References

[1] Abivin P, Hénaut I, Argillier J-F, Moan M. Viscosity behavior of foamy oil: Experimental study and modeling. Pet Sci Technol 2008;26(13):1545–58.

[2] Alshmakhy A, Maini BB. Foamy-oil-viscosity measurement. J Can Pet Technol 2012;51(01):60–5.

[3] Nemoto S, Kawata K, Kuribayashi T, Akiyama K, Kawai H, Murakawa H. A study of engine oil aeration. JSAE Rev 1997;18(3):271–6.

[4] Yang H-r, Wang X-L, Zhang Y-y, Du J-f. Study on the bubbly lubrication of journal bearings at various shear rates and temperatures. Tribol Int 2014;71:132–9.

[5] Farfan-Cabrera LI. Tribology of electric vehicles: A review of critical components, current state and future improvement trends. Tribol Int 2019;138:473–86.

[6] LePrince G, Changenet C, Ville F, Velex P, Dufau C, Jarnias F. Influence of aerated lubricants on gear churning losses–an engineering model. Tribol Trans 2011;54(6):929–38.

[7] ASTM International. ASTM D3427 - Standard test method for air release properties of hydrocarbon based oils. West Conshohocken, PA: ASTM International; 2019.

[8] International Organization for Standardization. ISO 12152:2012 Lubricants, industrial oils and related products — Determination of the foaming and air release properties of industrial gear oils using a spur gear test rig — Flender foam test procedure. Geneva: International Organization for Standardization; 2012.

[9] Chun SM. A parametric study on bubbly lubrication of high-speed journal bearings. Tribol Int 2002;35(1):1–13.

[10] Suja VC, Kar A, Cates W, Remmert S, Savage P, Fuller G. Evaporation-induced foam stabilization in lubricating oils. Proc Natl Acad Sci 2018;115(31):7919–24.

[11] Lorenceau E, Rouyer F. Lifetime of a single bubble on the surface of a water and ethanol bath. Phys Rev Fluids 2020;5(6):063603.

[12] Tran H-P, Arangalage M, Jørgensen L, Passade-Boupat N, Lequeux F, Talini L. Understanding frothing of liquid mixtures: A surfactantlike effect at the origin of enhanced liquid film lifetimes. Phys Rev Lett 2020;125(17):178002.

[13] Fowle T. Aeration in lubricating oils. Tribol Int 1981;14(3):151–7.

[14] Suzin Y, Ross S. Retardation of the ascent of gas bubbles by surface-active solutes in nonaqueous solutions. J Colloid Interface Sci 1985;103(2):578–85.

[15] Leroy V, Strybulevych A, Norisuye T. Time-resolved ultrasonic spectroscopy for bubbles. AIChE J 2017;63(10):4666–72.

[16] Leroy V, Strybulevych A, Page JH, Scanlon MG. Sound velocity and attenuation in bubbly gels measured by transmission experiments. J Acoust Soc Am 2008;123(4):1931–40.

[17] Garrett P, Davis J, Rendall H. An experimental study of the antifoam behaviour of mixtures of a hydrocarbon oil and hydrophobic particles. Colloids Surf A 1994;85(2–3):159–97.

[18] Bergeron V, Cooper P, Fischer C, Giermanska-Kahn J, Langevin D, Pouchelon A. Polydimethylsiloxane (PDMS)-based antifoams. Colloids Surf A 1997;122(1–3):103–20.

[19] Karakashev SI, Grozdanova MV. Foams and antifoams. Adv Colloid Interface Sci 2012;176:1–17.

[20] Denkov ND. Mechanisms of foam destruction by oil-based antifoams. Langmuir 2004;20(22):9463–505.

[21] Calhoun SG, Suja VC, Fuller GG. Foaming and antifoaming in non-aqueous liquids. Curr Opin Colloid Interface Sci 2021;101558.

[22] Liu H, Jurkschat T, Lohner T, Stahl K. Determination of oil distribution and churning power loss of gearboxes by finite volume CFD method. Tribol Int 2017;109:346–54.

[23] Maccioni L, Chernoray VG, Mastrone MN, Bohnert C, Concli F. Study of the impact of aeration on the lubricant behavior in a tapered roller bearing: Innovative numerical modelling and validation via particle image velocimetry. Tribol Int 2022;165:107301.